

# Controlling plasmonic Bloch modes on periodic nanostructures

B. Gjonaj,<sup>1,\*</sup> J. Aulbach,<sup>1</sup> P. M. Johnson,<sup>1</sup> A. P. Mosk,<sup>2</sup> L. Kuipers,<sup>1</sup> and A. Lagendijk<sup>1</sup>

<sup>1</sup>*FOM-Institute for Atomic and Molecular Physics AMOLF,  
Science Park 104, 1098 XG Amsterdam, The Netherlands*

<sup>2</sup>*Complex Photonic Systems, Faculty of Science and Technology,  
and MESA+ Institute for Nanotechnology, University of Twente,  
PO Box 217, 7500 AE Enschede, The Netherlands*

We study and actively control the coherent properties of Surface Plasmon Polaritons (SPPs) optically excited on a nano-hole array. Amplitude and phase of the optical excitation are externally controlled via a digital spatial light modulator (SLM) and SPP interference fringe patterns are observed with high contrast. Our interferometric observations reveal SPPs dressed with the Bloch modes of the periodic nano-structure. The momentum associated with these Dressed Plasmons (DP) is highly dependent on the grating period and fully matches our theoretical predictions. We show that the momentum of DP waves can in principle exceed the SPP momentum. Actively controlling DP waves via programmable phase patterns offers the potential for high field confinement applicable in sensing, Surface Enhanced Raman Scattering and plasmonic structured illumination microscopy.

Important systems such as biological cells, single molecules, and nanodevices, strongly interact with visible light on sub-wavelength scales. Yet standard microscopy and related applications in sensing and imaging are diffraction limited. Plasmonics [1] offers an alternative route to control light with sub-wavelength precision through the excitation of Surface Plasmon Polaritons (SPPs) [2, 3]. These surface waves, bound to a metal dielectric interface, are a hybrid mode of photons and electronic charge-density oscillations. The intrinsic momentum associated with these evanescent waves is higher than that of free propagating photons. Thus, for a fixed light frequency, SPPs have a higher effective refractive index and tighter confinement of electromagnetic energy [4].

Innovation in nano fabrication has enabled a remarkable degree of control over SPPs using metallic nanostructures. Specially tailored samples allow plasmonic waves to be coupled into the topological modes of a fabricated structure. The light field confinement, and therefore the resolution, addressed through the mode volume of these geometrically Dressed Plasmons (DP) exceeds by more than one order of magnitude that of standard SPP confinement. Successful geometries include coupled nanoantennas [5–7] that fully localize modes in the gap between neighboring antennas, and V-grooved [8, 9] and nanowire [10, 11] waveguides that support 1D propagating modes deeply confined inside the waveguide.

Yet there are limitations in using dressed plasmons for sensing applications. The electromagnetic field is only locally enhanced due to the fixed geometry of the structure yielding very high resolution but no field of view. Furthermore the specimen has to be inserted within the few nanometers width of the waveguide or the gap between nanoantennas, an extremely difficult task using current methods. However, theoretical works [12, 13] have shown that it is possible to use periodic nanostructures [14], such as well designed gratings [15], to support extended

DP waves to obtain both high resolution and large field of view. Furthermore, actively controlling these DP waves has the potential for plasmonic structured illumination microscopy [16] and related applications in imaging and sensing.

Here we show experimental observation and control of extended dressed plasmons supported by periodic nanostructures. Using a Spatial Light Modulator we shape the amplitude profile of the incident laser beam over a large 2D field of view. The SLM is imaged onto the surface of the sample thus addressing each pixel of the SLM to a corresponding area on the sample. This arrangement allows us to measure with high contrast fringe patterns generated from two counterpropagating SPP waves. Tuning the SLM phase pattern allows these fringes to be shifted and/or tilted at will. The momentum associated with the standing waves shows strong dependence on the lattice period of the grating and reveals the Bloch-mode dressing of the surface plasmons. Combining high momentum DP with focusing and scanning experiments [17] has the potential to revolutionize far field bio-sensing applications.

A diagram of the setup is given in Fig. 1. The SLM is imaged on the sample via a lens ( $L_1$ ) and the objective, referred to hereafter together as the imaging system. The SLM is at the focal plane of lens  $L_1$  (focal length 130 cm). The image at infinity created by  $L_1$  is projected onto the sample at the focal plane of the objective. Our SLM (Holoeye LC-R 720) is a reflective display based on Twisted Nematic Liquid Crystal on Silicon technology. The display has a total of 1280 x 768 pixels operating at 60 Hz with a response time of 3 ms. Each pixel is 20  $\mu\text{m}$  in size and addressed with a 8-bit voltage. The objective (Nikon LU PLAN FLUOR P 100X) is infinity corrected and metallurgic (no coverslip compensation) with a Numerical Aperture (NA) of 0.9 and a magnification of 100 times (defined for a tube lens of 20 cm focal length). The focal length of  $L_1$  is 6.5 times larger than that of the standard tube lens yielding a corresponding 650 times demag-

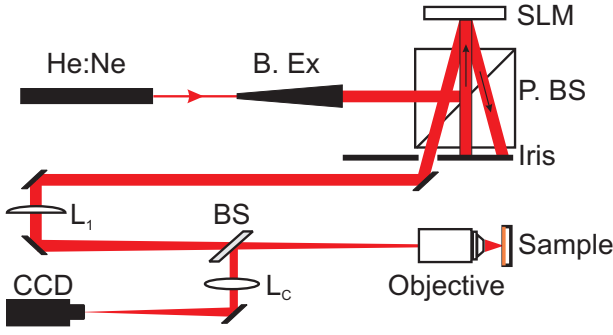


FIG. 1. Experimental Setup. The Spatial Light Modulator (SLM) is projected onto the sample via the imaging system (lens  $L_1$ , objective). The sample is imaged on the CCD camera via the system (objective, lens  $L_C$ ). The abbreviations B. Ex, BS and P. BS stand for beam expander, beam splitter and polarizing beam splitter respectively. Inset: SEM image ( $5 \times 5 \mu\text{m}$ ) of 450 nm nanohole array.

nification of the image. The distance between  $L_1$  and the objective is 1 m i.e. smaller than the focal length of  $L_1$  (non-telecentric imaging system). In this configuration the average angle of illumination is position dependent, which is an important condition for the SPPs launching.

The light emitted in reflection from the sample is imaged on the CCD (AVT Dolphin F145 B) using lens  $L_C$  as tube lens. This light includes both the direct reflection of the illuminating beam and the scattered light from SPPs. Thus the resulting image is a combination of both the SLM amplitude pattern and the generated SPP pattern. To distinguish between the two we choose illumination patterns that allow SPP observation in a non-illuminated area. The amplitude and phase of the excitation pattern is controlled by applying the 4-pixel technique [18] to the SLM. Four adjacent pixels are grouped into a superpixel by selecting a first diffractive order with the neighbor-pixel fields being  $\pi/4$  out of phase. In this work we use  $32 \times 32$  superpixels. Every SLM superpixel is imaged on a sample area of  $440 \times 440 \text{ nm}^2$  containing nearly one unit cell of the grating. Such a superpixel grouping provides continuous modulation over full amplitude ( $A \in [0, 1]$ ) and phase ( $\Phi \in [0, 2\pi]$ ) ranges with a cross modulation of less than 1%.

Our samples, nanohole arrays similar to those used typically for Enhanced Optical Transmission experiments, were fabricated using focused ion beam milling. A 200 nm gold film was deposited on top of 1 mm BK7 glass substrate with a 2 nm chromium adhesion layer. Square holes were milled with sides of 177 nm. The hole array covers an area of  $30 \times 30 \mu\text{m}^2$ . Five samples were fabricated with array periods ( $a_0$ ) varying from 350 nm to 450 nm. The sample was placed with the gold side towards the objective to observe SPP waves from the gold-air interface. We calculate the SPP momentum for

incident radiation of  $\lambda_0 = 633 \text{ nm}$  ( $k_0 = 2\pi/\lambda_0$ ) using tabulated values [19] of the dielectric constants of gold  $\epsilon_m$  and air  $\epsilon_d$

$$k_S = k_0 \text{Re} \sqrt{\frac{\epsilon_m \epsilon_d}{\epsilon_m + \epsilon_d}} = (m, n)k_G + k_0 \sin \theta, \quad (1)$$

where the last equality expresses the fact that the SPP momentum is a vectorial sum of the  $(m, n)k_G$  grating orders ( $k_G = 2\pi/a_0$ ) and the in-plane component of the incident light. With our oblique illumination scheme, the average angle of incidence  $\theta$  is not uniform but position dependent.

This illumination scheme and its role on how SPPs are launched is illustrated in Fig. 2. Each SLM's superpixel is projected onto the sample with a different average angle of incidence (Fig. 2a) and thus with a different in-plane component of the incident light. The momentum conservation described in Eq. 1 will be satisfied only within specific angular bands which are position dependent. In Fig. 2b-d we show the surface of three different samples illuminated with a uniform amplitude profile across the SLM with horizontal polarization.

For the reference bare gold film and a uniform SLM amplitude and phase profile, the reflected image is identical to incident beam profile since no SPP can be launched (Fig. 2b). When the same uniform amplitude and phase profile is projected onto a nanohole array, dark and bright areas are clearly distinguishable as shown in Fig. 2c-d. Dark areas correspond to suppressed reflection from the sample. We interpret these dark areas as the spatial (angular) bands that satisfy Eq. 1 and thus where plasmons

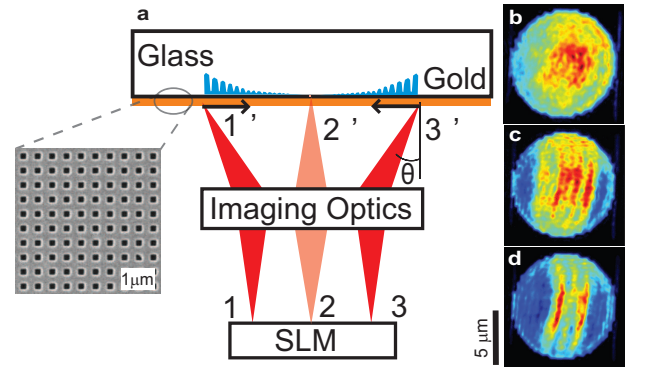


FIG. 2. (a) Sketch of the sample illumination. Each SLM point is imaged on the surface of the sample with a different average angle of incidence  $\theta$ . (b-d) Reflection from different samples illuminated with a uniform amplitude and phase profile. (b) On the bare gold sample the reflection is also uniform since no SPPs are launched. (c) The dark areas of low reflection from the 400 nm hole array indicate the angular (spatial) bands for SPP launching. (d) These bands are sample dependent as shown for the 425 nm hole array. Inset: SEM image of the samples.

are efficiently excited from the incident light. The location of these bands strongly depends on the array momentum. Even a 25 nm variation of the array period from  $a_0 = 425$  nm (Fig. 2c) to  $a_0 = 400$  nm (Fig. 2d) yields a spatial band shift of nearly  $2 \mu\text{m}$ .

SPPs waves launched in the momentum matched bands propagate towards each other and interfere (Fig. 2). Yet this interference pattern is observed on a high background due to the direct reflection of the incident light. To remove the background and enhance the contrast of the SPP interference pattern we spatially design the incident amplitude profile with “on” areas of amplitude  $A = 1$  and an “off” background of  $A = 0$ . Each “on” area is composed of  $10 \times 8$  superpixels and is located in the vicinity of the two symmetric angular bands. The SPP interference patterns are then observed in the central non-illuminated area which is our SPP field of view.

Results from this designed amplitude profile are shown in Fig. 3. When the two counterpropagating SPP waves launched in the “on” areas interfere, a standing wave pattern of intensity is created. For SPPs propagating on an ideally smooth and non-corrugated sample we expect the period of the fringe pattern to be half the SPP wavelength

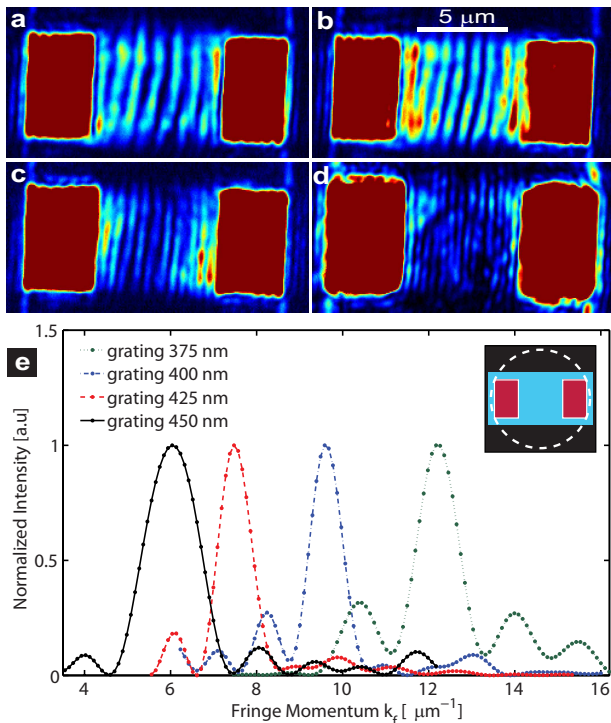


FIG. 3. SPP fringe formation via counter propagating waves. The image geometry and the incident amplitude profile are shown in the inset. The polarization of the incident light is horizontal. (a-d) we observe different fringe patterns for array periods of 375 nm (a), 400 nm (b), 425 nm (c) and 450 nm (d). In (e) are shown the line Fourier transforms of these fringe patterns.

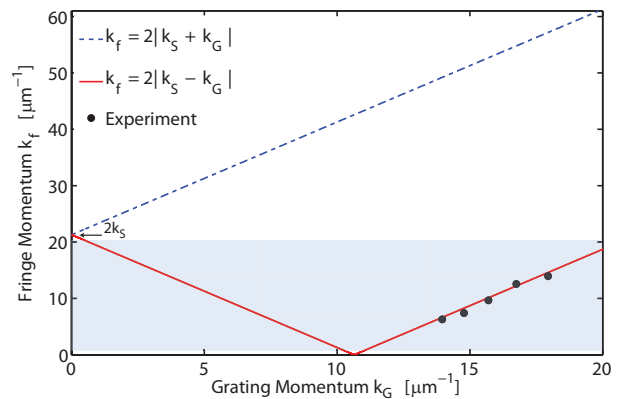


FIG. 4. SPP fringe momentum versus the grating momentum. The experimental data shows SPPs convoluted with the  $m = -1$  Bloch mode of the arrays. The other Bloch modes can not be resolved due to limited detection bandwidth (light blue square).

( $\lambda_S = 2\pi/k_S = 590\text{nm}$ ). Instead, the measured fringe period is found to be sample dependent (Fig. 3a-d). We measured fringe periods  $P$  of  $1 \pm 0.05 \mu\text{m}$ ,  $0.85 \pm 0.05 \mu\text{m}$ ,  $0.65 \pm 0.05 \mu\text{m}$ ,  $0.5 \pm 0.05 \mu\text{m}$  and  $0.45 \pm 0.05 \mu\text{m}$  for grating pitches of 450 nm, 425 nm, 400 nm, 375 nm and 350 nm respectively. The different filling fractions of our samples, that perturb the SPP wavelength within few percent, can not explain the large deviations we observe.

We attribute the fringe patterns to a mixing of the original SPP wave with the hole array [20]. We can analyze the results using a one dimensional model because for all our samples we observe only horizontal propagation. Theoretically there are two ways to mix SPPs with the hole array: intensity mixing (expected for incoherent forms of scattering such as fluorescence) and field convolution (expected for coherent scattering processes). We will discuss both ways even though the experimental observations confirm only the field convolution. We first consider intensity convolution: a SPP standing intensity pattern with momentum  $2k_S$  is formed, but since we observe the pattern through the scattering of a periodic structure with momentum  $k_G$ , the fringe momentum appears to be  $2k_S \pm k_G$ . This intensity convolution does not match the experimental observations. The situation is completely different for the field convolution: the hybridization of the bare SPPs with the Bloch modes of the array results in dressed plasmonic (DP) waves of momentum  $k_S + m \cdot k_G$  ( $m$  integer). These DP waves then result in standing intensity patterns of momentum  $2(k_S + m \cdot k_G)$ .

A comparison between experiment and the amplitude convolution approach for these DP waves is shown in Fig. 4. The modulus of the fringe momentum ( $k_f$ ) is plotted against the module of the grating momentum ( $k_G$ ). The two lines are the theoretical predictions for SPPs convoluted with the first positive ( $m = 1$ ) and the

first negative ( $m = -1$ ) grating orders. The experimental data perfectly follow only the  $m = -1$  curve. The first positive order is not observed in our far field measurement due to its evanescent non-radiative nature and the limited resolution of our setup. The distribution of fringe momenta can be expressed except for a normalization factor as

$$P_f(k) = B(k) \sum_{m \in \mathbb{Z}} \eta_m \cdot \delta(k - 2|k_S + mk_G|), \quad (2)$$

where every delta represents the standing pattern from one of the  $m$  orders of the array,  $\eta_m$  represents the coupling efficiency of SPPs into this  $m$ -th order and  $B(k)$  is the momentum bandwidth of our detection optics. Our bandwidth is shown as the light blue quadrature in Fig. 4 and we approximate it with a step function limited by the optical diffraction limit and the SPP field of view (the distance between the two “on” areas). Upon inserting this bandwidth in Eq. 2 only SPP hybridization with the  $m = -1$  term survives because all other DP modes have fringe momentum that exceeds the diffraction limit.

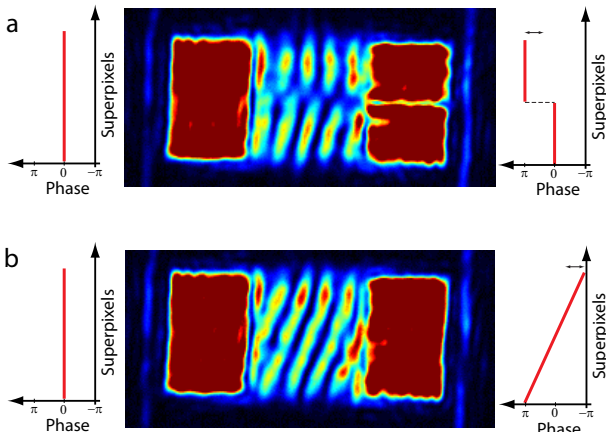


FIG. 5. Scanning the fringes by phase tuning. (a) The phase of the left “on” area is kept constant while the phase of the right “on” area has a step jump between the lower and upper part as shown in the wings of the figure. The resulting fringe pattern in the upper part is shifted compared to the lower one. (b) The fringes are rotated due to a linearly increasing phase on the right “on” area.

We can scan the fringe pattern across the sample by varying the phase delay between the two “on” areas and thus introducing an optical retardation that will translate the DP fringes. We experimentally prove this phase scanning principle for the  $m = -1$  DP modes as shown in Fig. 5a where the upper half of the right “on” area is out of phase with the rest of the illuminated areas. The different phase delays result in a translated fringe pattern in the upper part. The line scan resolution (fringe translation) is given by our digital phase control: 256 steps from 0 to  $2\pi$  phase delay. In alternative, by applying a linear phase difference between the two “on” areas, the

standing pattern will result in tilted plasmonic fringes (angular scan) as shown in Fig. 5b.

The predicted presence of the  $m = 1$  DP mode, which represents a sub 100 nm period intensity beating on top of the observed fringe pattern, combined with our ability to scan the pattern across the sample, suggest interesting prospects for subwavelength imaging. Due to the diffraction limit we can not resolve this fast beating in the current setup. However it should be possible, using near field imaging, to calibrate this sub 100 nm intensity pattern for different fringe patterns (line and angular scans). Once calibrated, the sample surface could be used to image sub 100 nm objects with only far field probing and image correlations.

We have shown here the observation of Bloch-mode dressed surface plasmon polaritons (DP) propagating on nanohole arrays of different subwavelength periodicities. We recorded the standing intensity pattern of two counterpropagating DP waves. The dependence of the measured fringe period on the period of the nano structure is perfectly described by a simple model of plasmonic Bloch mode interference. By actively imposing well programmed phase relations to these plasmonic Bloch modes we achieved full control of their interference fringe patterns. Bloch dressed SPPs are 2D propagating waves that can achieve high momentum and thus actively controlling their interference patterns has potential for super-resolution biosensing and imaging applications.

## ACKNOWLEDGMENTS

We thank Hans Zeijlrmaker and Dimitry Lamers for sample fabrication. This work is part of the research program of the “Stichting voor Fundamenteel Onderzoek der Materie”, which is Financially supported by the “Nederlandse Organisatie voor Wetenschappelijk Onderzoek”.

\* b.gjonaj@ee.technion.ac.il; Current address: Technion Israel Institute of Technology

- [1] W. L. Barnes, A. Dereux, and T. W. Ebbesen, *Nature* **424**, 824 (2003).
- [2] E. Ozbay, *Science* **311**, 189 (2006).
- [3] A. Polman, *Science* **322**, 868 (2008).
- [4] J. A. Schuller, E. S. Barnard, W. Cai, Y. C. Jun, J. S. White, and M. L. Brongersma, *Nat. Mater.* **9**, 193 (2010).
- [5] P. J. Schuck, D. P. Fromm, A. Sundaramurthy, G. S. Kino, and W. E. Moerner, *Phys. Rev. Lett.* **94**, 017402 (2005).
- [6] P. Mühlischlegel, H. J. Eisler, O. J. F. Martin, B. Hecht, and D. W. Pohl, *Science* **308**, 1607 (2005).
- [7] L. Novotny and N. van Hulst, *Nat. Photon.* **5**, 83 (2011).

- [8] T. Sndergaard, S. I. Bozhevolnyi, J. Beermann, S. M. Novikov, E. Devaux, and T. W. Ebbesen, *Nano Lett.* **10**, 291 (2010).
- [9] M. I. Stockman, *Phys. Rev. Lett.* **93**, 137404 (2004).
- [10] J. R. Krenn, B. Lamprecht, H. Ditlbacher, G. Schider, M. Salerno, A. Leitner, and F. R. Aussenegg, *EPL (Europhys. Lett.)* **60**, 663 (2002).
- [11] E. Verhagen, M. Spasenović, A. Polman, and L. K. Kuipers, *Phys. Rev. Lett.* **102**, 203904 (2009).
- [12] A. Sentenac and P. C. Chaumet, *Phys. Rev. Lett.* **101**, 013901 (2008).
- [13] G. Bartal, G. Lerosey, and X. Zhang, *Phys. Rev. B* **79**, 201103 (2009).
- [14] T. S. Kao, S. D. Jenkins, J. Ruostekoski, and N. I. Zheludev, *Phys. Rev. Lett.* **106**, 085501 (2011).
- [15] S. G. Rodrigo, O. Mahboub, A. Degiron, C. Genet, F. J. García-Vidal, L. Martín-Moreno, and T. W. Ebbesen, *Opt. Express* **18**, 23691 (2010).
- [16] F. Wei and Z. Liu, *Nano Lett.* **10**, 2531 (2010).
- [17] B. Gjonaj, J. Aulbach, P. M. Johnson, A. P. Mosk, L. Kuipers., and A. Lagendijk, *Nat. Photon.* **5**, 360 (2011).
- [18] E. G. van Putten, I. M. Vellekoop, and A. P. Mosk, *Appl. Opt.* **47**, 2076 (2008).
- [19] P. B. Johnson and R. W. Christy, *Phys. Rev. B* **6**, 4370 (1972).
- [20] D. S. Kim, S. C. Hohng, V. Malyarchuk, Y. C. Yoon, Y. H. Ahn, K. J. Yee, J. W. Park, J. Kim, Q. H. Park, and C. Lienau, *Phys. Rev. Lett.* **91**, 143901 (2003).